Downward wave coupling between the stratosphere and troposphere: The importance of meridional wave guiding and comparison with zonal-mean coupling

Tiffany A. Shaw *

Center for Atmosphere Ocean Science, Courant Institute of Mathematical Sciences,

New York University, New York, New York, USA

Judith Perlwitz

Cooperative Institute for Research in Environmental Sciences, University of Colorado/

NOAA Earth System Research Laboratory, Physical Sciences Division, Boulder, Colorado, USA

Nili Harnik

Deprtment of Geophysics and Planetary Sciences,

Tel Aviv University, Tel Aviv, Israel.

* *Corresponding author address:* Dr. Tiffany A. Shaw, Center for Atmosphere Ocean Science, Courant Institute of Mathematical Sciences, New York University, 251 Mercer St., New York, NY 10012.

E-mail: tshaw@cims.nyu.edu

ABSTRACT

The nature of downward wave coupling between the stratosphere and troposphere in both hemispheres is analyzed using the ERA-40 reanalysis data set. Downward wave coupling occurs when planetary waves reflected in the stratosphere impact the troposphere and is distinct from zonal-mean coupling, which results from wave dissipation and its subsequent impact on the zonal-mean flow. Using a cross-spectral correlation analysis and wave geometry diagnostics, we find that downward wave-one coupling occurs in the presence of both a vertical reflecting surface in the mid-to-upper stratosphere and a high-latitude meridional wave guide in the lower stratosphere. In the southern hemisphere downward wave coupling occurs from September to December, while in the northern hemisphere it occurs from January to March. A vertical reflecting surface is also present in the stratosphere during early winter in both hemispheres, however it forms at the poleward edge of the meridional wave guide, which is not confined to high latitudes. The absence of a high-latitude wave guide allows meridional wave propagation into the subtropics and decreases the likelihood of downward wave coupling. The results highlight the importance of distinguishing between wave reflection in general, which requires a vertical reflecting surface, and downward wave coupling between the stratosphere and troposphere, which requires both a vertical reflecting surface and a high-latitude meridional wave guide.

The relative roles of downward wave and zonal-mean coupling in the southern and northern hemispheres are subsequently compared. In the southern hemisphere, downward wave-one coupling dominates, while in the northern hemisphere downward wave-one coupling and zonal-mean coupling are found to be equally important from winter to early spring. The results suggest that an accurate representation of the seasonal cycle of the wave geometry is

necessary for the proper representation of downward wave coupling between the stratosphere and troposphere.

1. Introduction

Planetary waves represent the most important source of dynamical coupling between the stratosphere and troposphere. They are generated in the troposphere by orography and continent-ocean heating asymmetries and propagate upward into the stratosphere where they either dissipate and initiate a downward propagating zonal-mean response or they are reflected downward towards the troposphere. The focus of many recent studies has been on zonal-mean stratosphere-troposphere coupling (e.g., Baldwin and Dunkerton 2001; Thompson et al. 2005). This type of coupling has been shown to be important for seasonal prediction in the troposphere during northern hemisphere winter (Baldwin et al. 2003). Wave reflection in the stratosphere, which impacts the troposphere (called downward wave coupling), is another important source of dynamical coupling, however its intraseasonal impact has not been extensively studied.

In the northern hemisphere, Perlwitz and Harnik (2003) showed that significant downward wave-one coupling between the stratosphere and troposphere occurs during January, February and March (JFM). They used a time-lagged singular value decomposition analysis to isolate downward propagating wave-one signals and found statistically significant correlations for time lags when wave one patterns in the stratosphere lead those in the troposphere. The wave reflection signal coincided with a vertical reflecting surface (a region of negative vertical wavenumber) in the stratosphere above 10 hPa. The vertical reflecting surface was diagnosed using the wave geometry diagnostic of Harnik and Lindzen (2001). In Perlwitz and Harnik (2003) the JFM period was contrasted with September, October and November (SON) in the northern hemisphere, which did not show significant wave one correlations

between stratospheric and tropospheric levels for time lags when the stratosphere lead the troposphere. The lack of downward wave coupling in SON was consistent with the wave geometry diagnostic, which showed no reflecting surface during that time.

In the southern hemisphere, Randel (1987) noted wave reflection in his study of planetary wave propagation for two 120 day winter seasons (June 1 to September 28 1983 and 1984). He used a cross-spectral correlation analysis to study the vertical propagation of planetary waves. The upward propagation time scales from this analysis method agree with those from the time-lagged singular value decomposition analysis used by Perlwitz and Harnik (2003). In the winter of 1983, Randel (1987) found significant correlations for time lags when the stratosphere lead the troposphere. These correlations coincided with downward pointing Eliassen-Palm vectors in the lower stratosphere (Randel et al. 1987). However, the cause of the wave reflection was not studied in detail because the focus of the study was on upward propagating waves, which represent the dominant signal. Harnik and Lindzen (2001) used their wave geometry diagnostic to show that a vertical reflecting surface forms towards late winter as part of the climatological seasonal cycle in the southern hemisphere, however the impact on the troposphere was not discussed. Overall much less is known about downward wave coupling in the southern hemisphere.

These previous studies provide observational evidence for downward wave coupling between the stratosphere and troposphere in both hemispheres during the winter season. They highlight the importance of a vertical reflecting surface as a condition required for wave reflection. Here we explore the seasonal cycle of downward wave-one coupling between the stratosphere and troposphere. We show that downward wave coupling only occurs during those times of the year with a particular wave geometry, which involves both a vertical reflect-

ing surface and a high-latitude meridional wave guide. This leads to a distinction between wave reflection in general, which requires a vertical reflecting surface in the stratosphere, and downward wave coupling between the stratosphere and troposphere, which requires both a vertical reflecting surface and a high-latitude meridional wave guide.

We subsequently investigate the relative roles of zonal-mean and downward wave coupling between the stratosphere and troposphere in the seasonal cycle of both hemispheres. Recent studies have pointed to non-zonal decadal variability and trends in the southern hemisphere troposphere and stratosphere (Neff et al. 2008; Lin et al. 2009). Perlwitz and Harnik (2004) showed that winters (i.e. JFM) in the northern hemisphere are either reflective and characterized by downward wave-one coupling or non-reflective and characterized by zonal-mean coupling. Understanding the roles of zonal-mean and downward wave coupling in the seasonal cycle is important for understanding atmospheric variability and its response to climate change. A better characterization of dynamical coupling between the stratosphere and troposphere on intraseasonal timescales is also important for model validation. Only models with a proper representation of both zonal-mean and wave coupling can be used to assess the impact of the stratosphere on tropospheric climate and climate change, which is an important topic of current research (Shaw and Shepherd 2008).

Section 2 describes the reanalysis data set and analysis methods used in this study. In sections 3 we investigate downward wave coupling in the southern and northern hemispheres. In section 4 we assess the relative roles of zonal-mean and downward wave coupling during the seasonal cycle in the southern and northern hemispheres. The paper concludes with a summary and discussion in section 5.

2. Data and analysis approach

The data used in this study are the daily three-dimensional geopotential, monthly-mean zonal-mean zonal wind and temperature fields from the ECMWF ERA-40 reanalysis data set covering the period from January 1979 to August 2002 (Uppala et al. 2005). As noted by Harnik and Lindzen (2001) and Perlwitz and Harnik (2003), vertical reflecting surfaces in both the southern and northern hemispheres typically form above 10 hPa. The ERA-40 data set was chosen because it extends from the surface to 1 hPa and has a good representation of the stratosphere. In the analysis that follows, all of the ERA-40 results were found to be in good agreement with the results from the Modern Era Restrospective-analysis for Research and Application (MERRA) reanalysis and the Japanese 25-year Reanalysis Project (JRA-25) data sets and are therefore robust.

To isolate the upward and downward propagating planetary wave signals we use the cross-spectral correlation diagnostic of Randel (1987). The diagnostic considers two geopotential height Fourier coefficients of wavenumber k at two different latitudes and heights

$$Z_{1_k} = S_{1_k}(t)\sin(kx) + C_{1_k}(t)\cos(kx), \tag{1}$$

$$Z_{2_k} = S_{2_k}(t)\sin(kx) + C_{2_k}(t)\cos(kx) \tag{2}$$

and determines their in-phase and out-of-phase correlations

$$CO = \langle S_{1_k}, S_{2_k}\rangle_\tau + \langle C_{1_k}, C_{2_k}\rangle_\tau, \qquad QD = \langle S_{1_k}, C_{2_k}\rangle_\tau + \langle C_{1_k}, S_{2_k}\rangle_\tau \tag{3}$$

where

$$\langle S_{1_k}, S_{2_k}\rangle_\tau = \frac{\frac{1}{N-\tau}\sum_{t=1}^{N-\tau} S_{1_k}(t)\cdot S_{2_k}(t+\tau)}{\sigma_{Z_{1_k}}\cdot\sigma_{Z_{2_k}}} \tag{4}$$

is the linear correlation at time lag τ between $S_{1_k}(t)$ and $S_{2_k}(t)$ and $\sigma_{Z_{1_k}}$ ($\sigma_{Z_{2_k}}$) is the square root of the variance of $Z_{1_k}(x,t)$ ($Z_{2_k}(x,t)$). The in-phase and out-of-phase correlations are then used to compute the correlation coherence and correlation phase for the two wave coefficients:

$$coh = \sqrt{CO^2 + QD^2}, \quad ph = \arctan(-QD/CO). \tag{5}$$

The correlation coherence and phase are used to understand the co-relation between a wave at a given reference level (in the troposphere or stratosphere) with other levels in the vertical as a function of time lag. Here we focus on zonal wavenumber one and use a reference latitude band from 45 to 80 degrees and a reference level at 500 hPa in both hemispheres.[1] We choose to average wave one over a reference latitude band, rather than consider a specific latitude, to account for the change in position of the maximum heat flux throughout the seasonal cycle. Note that the correlation coherence and phase do not provide any information about the zonal propagation of the wave. However, correlations at sufficiently small time lags likely reflect the stationary component. We high-pass filter the wave signals to remove variability greater than a year so as to focus on intraseasonal variability. The upward propagating wave-one signal is identified by statistically significant correlations for time lags when the reference wave one field at 500 hPa leads the wave field at levels in the stratosphere. Here we are interested in the downward propagating wave-one signals (associated with wave reflection), which are identified by significant correlations for time lags when the reference wave field lags the wave field at levels in the stratosphere. Upward or downward wave propagation

[1]We focus on zonal wave one because it represents the dominant source of downward wave coupling. We also found evidence for downward wave-two coupling in the southern hemisphere, however it is much weaker than wave-one coupling.

is confirmed using the correlation phase: upward (downward) propagating waves have a westward (eastward) phase tilt with height. Further details regarding the cross-spectral correlation diagnostic can be found in section 2b of Randel (1987).

The second analysis technique used is the wave geometry diagnostic of Harnik and Lindzen (2001). The diagnostic separates the more commonly used index of refraction (c.f. Charney and Drazin 1961) into vertical (m) and meridional (l) wavenumber contributions. The wavenumbers are diagnosed from the solution to the wave equation associated with the conservation of potential vorticity in spherical coordinates linearized about a zonal-mean basic state (presented here for illustrative purposes in Cartesian coordinates):

$$\frac{\partial^2\psi}{\partial z^2} + \frac{N^2}{f^2}\frac{\partial^2\psi}{\partial y^2} + n_{ref}^2\psi = 0 \tag{6}$$

where ψ is the weighted wave geopotential height, z and y are the vertical and meridional coordinates, N^2 and f are the zonal-mean basic state Brunt-Väisälä frequency and Coriolis parameter and

$$n_{ref}^2 \equiv \frac{N^2}{f^2}\left\{\frac{\overline{q}_y}{U-c} - k^2 + f^2\frac{e^{z/2h}}{N}\frac{\partial}{\partial z}\left[\frac{e^{-z/h}}{N}\frac{\partial}{\partial z}(e^{z/2h}N)\right]\right\} = m^2 + \frac{N^2}{f^2}l^2 \tag{7}$$

is the squared index of refraction with U, $\overline{q}_y$ the basic state zonal-mean zonal wind and meridional potential vorticity gradient, c is the wave phase speed and h is the scale height. The last equality in (7) is the corresponding dispersion relation. Here we focus on zonal wavenumber one and set $c = 0$, i.e. we consider stationary wave one. The coefficients of the wave equation (6) are calculated using monthly-mean zonal-mean zonal wind and temperature data. The vertical and meridional wavenumbers are subsequently diagnosed from the solution to the wave equation:

$$\mathrm{Re}\left(\frac{\psi_{zz}}{\psi}\right) = -m^2, \quad \mathrm{Re}\left(\frac{\psi_{yy}}{\psi}\right) = -l^2 \tag{8}$$

where Re denotes the real part. The separation into vertical and meridional wavenumbers distinguishes between regions which represent barriers for vertical and meridional propagation. As for the squared index of refraction, waves propagate in the vertical direction when $m^2 > 0$, are evanescent when $m^2 < 0$ and are reflected when $m^2 = 0$. Similarly, waves propagate in the meridional direction when $l^2 > 0$, are evanescent when $l^2 < 0$ and are reflected when $l^2 = 0$. The wave geometry diagnostic is used to determine whether the basic state for a given month in the seasonal cycle is reflective in the vertical and meridional directions. Further details can be found in Harnik and Lindzen (2001).

3. Downward wave coupling and meridional wave guiding

a. Southern hemisphere

We examine downward wave coupling in the southern hemisphere by considering wave-one propagation in two month overlapping periods from April to December. Figure 1 shows the wave-one cross-correlations with a reference latitude band from 45 to 80°S at 500 hPa with vertical levels from 1000 to 1 hPa for time lags between -10 and 10 days. Correlations which exceed 0.18 are statistically significant at the 99% level and only significant correlations are contoured in Fig 1. Since the reference level is in the troposphere, positive lags have the troposphere leading the stratosphere where as negative lags have the stratosphere leading the troposphere. The correlations only reflect intraseasonal variability since we have removed variability greater than one year as discussed in section 2. According to the cross-

correlations there is significant upward propagation (significant correlations for positive lags) from April to December. The upward propagation time from 500 to 5 hPa varies throughout the seasonal cycle from 3 to 4 days in agreement with Randel (1987). The correlations are very weak during November-December which is expected because of the transition to westward zonal winds and the formation of a critical surface for stationary wave one, i.e. where the zonal wind equals zero (Charney and Drazin 1961). Figure 2 shows the vertical phase structure in May-June (left panel) and October-November (right panel) for +4 day lag (dashed line), which corresponds to the time lag when the correlations maximize in the stratosphere. The upward propagation for positive lags is confirmed by the vertical phase structure from representative two-month periods. The phase tilt is westward with height above 500 hPa in both May-June and October-November, which indicates upward wave propagation.

While there is significant upward propagation during most of the year, there are only significant correlations for downward propagation (i.e. for negative lags) from September to December. The correlations for negative lags maximize in October-November. The downward propagation time from 5 to 500 hPa is approximately 4 days. Figure 2 shows that the phase tilt for the -4 day lag correlation (solid line) is eastward with height above 500 hPa in both May-June and October-November, which confirms that the negative time lags are associated with downward wave propagation. In October-November there is a very large eastward phase tilt between 200 and 100 hPa and the tilt in the stratosphere is very small. A similarly large westward phase tilt between 200 and 100 hPa is found for the upward propagating wave pattern (Fig. 2 dashed line, right panel). The combined phase structure of the upward and downward propagating waves is suggestive of a vertical standing wave

and is indicative of a wave in the presence of a permanent vertical reflecting surface. The phase tilt with height in May-June is much smoother and is not suggestive of a standing wave pattern.

In order to better understand the nature of downward wave coupling throughout the seasonal cycle we consider the evolution of the wave geometry. Figure 3 shows the climatological seasonal cycle of the zonal wave-one vertical wavenumber (m) averaged between 55 and 75°S (top panel) along with zonal-mean cross sections of the vertical wavenumber during May-June (bottom left panel) and October-November (bottom right panel). The shading indicates regions of wave evanescence, which are bounded by the $m = 0$ surface, called a vertical reflecting surface. The solid line indicates the $m = 0.01$ m^{-1} surface. The dashed lines indicate regions where $m = 2, 4$ m^{-1}, i.e. where m is small. It is clear from the seasonal cycle of the vertical wavenumber that there are two times during the year when there is a vertical reflecting surface in the stratosphere: early winter (May to July) and late spring (September to November). Evidently, the evanescent (shaded) region below 100 hPa from March to September is too narrow (much smaller than a vertical wavelength) to block upward wave propagation since the cross correlations for positive lags are large during that time (see Fig. 1). The reflecting surface during October-November extends further toward the equator than the vertical reflecting surface in May-June, which is confined toward the pole. Note that the lowering of the evanescent region from October to January is consistent with the formation of a critical surface for planetary waves discussed previously.

The climatological seasonal cycle of the vertical wavenumber suggests that there should be wave reflection in both May-June and October-November. However, the cross-correlations only show statistically significant downward wave coupling during the latter period. The

two diagnostics suggest that a vertical reflecting surface is not sufficient for downward wave coupling between the stratosphere and troposphere. We thus examine the second wave geometry diagnostic, which is the meridional wavenumber. Figure 4 shows the seasonal cycle of the zonal wave-one meridional wavenumber (l) averaged between 100 and 10 hPa (top panel) along with zonal-mean cross sections of the meridional wavenumber during May-June (bottom left panel) and October-November (bottom right panel). The dark shaded regions represent regions of wave evanescence bounded by the $l = 0$ surface, which represent a boundary to meridional propagation. The solid line indicates the $l = 0.01$ rad^{-1} surface. We see that meridional propagation is confined to a specific latitudinal region, which we refer to as the meridional wave guide. Overlying the seasonal cycle of l is the seasonal cycle of m averaged between 10 to 1 hPa. The lighter shaded regions represent regions of vertical wave evanescence and the dashed line represents the $m = 0.01$ m^{-1} surface. In the bottom panels of Fig. 4 we also include the shading representing vertical wave evanescence and the $m = 0.01$ m^{-1} surface, which is identical to the solid lines in the bottom panels of Fig. 3. Figure 4 clearly indicates that throughout most of the seasonal cycle (January to August) there is a very wide meridional wave guide (the north and south evanescent regions are separated by 30 to 40 degrees of latitude). This wide meridional wave guide allows waves to propagate equatorward into the subtropical region where they would encounter a subtropical critical surface, which extends to the equatorward boundary of the wave guide. From September to December however, there is a high-latitude meridional wave guide from approximately 40 to 70°S. Thus, unlike the case for the vertical wavenumber, there is a clear difference in the meridional wavenumber between the May-June and October-November periods.

The combined l and m seasonal cycles in Fig. 4 reveal that from October to December

the high-latitude meridional wave guide is bounded above by a vertical reflecting surface. This configuration forms a bounded wave geometry (cf. the October-November zonal-mean cross section, Fig. 4 bottom right panel), and coincides with the maximum downward wave coupling in Fig. 1. In contrast, the wave geometry during May-June is not bounded (Fig. 4 bottom left panel). In particular, there is no high-latitude meridional wave guide and thus the waves can propagate meridionally into the subtropics instead of propagating vertically. Even if the waves were to propagate vertically the vertical reflecting surface does not extend far enough equatorward to induce wave reflection. As a result, there is no significant downward wave coupling during May-June.

The hypothesis is that the absence of a high-latitude meridional wave guide in May-June results in more meridional wave propagation instead of strict vertical propagation. A high-latitude wave guide acts to guide vertically propagating waves upward toward the vertical reflecting surface, which increases the likelihood of downward wave coupling. To confirm that meridional wave guiding is important for guiding vertically propagating planetary waves we consider the seasonal cycle of wave-one Eliassen-Palm (EP) fluxes. Figure 5 shows the climatological seasonal cycle of the ratio of the meridional component of the wave-one EP flux at 35°S averaged between 100 and 10 hPa to the vertical flux at 100 hPa averaged between 35 and 90°S (solid line) from June to December. The ratio quantifies how much of the wave-one activity flux entering the stratosphere at 100 hPa between 35 and 90°S propagates equatorward. It has a clear negative trend and decreases by a factor of three between May-June and October-November. This confirms that there is significant meridional propagation in June to August, which is consistent with the lack of a high-latitude meridional wave guide during that time. The meridional propagation is significantly decreased from September to

November, which is consistent with the presence of a high-latitude meridional wave guide. Figure 5 also shows the ratio between the vertical flux at 10 hPa and the vertical flux at 100 hPa both averaged between 35 and 90°S (dashed line). This ratio quantifies how much of the wave-one activity flux entering the stratosphere at 100 hPa between 35 and 90°S propagates vertically through the stratosphere and reaches 10 hPa. The ratio peaks during mid-winter (August-September) at the time when there is no reflecting surface. This also agrees with the seasonal evolution of the wave geometry. Note that the sum of the two EP ratios exceeds one during certain times, which suggests the stratosphere is a source of wave one during these times of the year. Randel et al. (1987) noted a wave source in the upper troposphere (between 300 to 100 hPa). These EP flux ratio diagnostics support the hypothesis that a bounded wave geometry, particularly in the meridional direction, is important for preventing meridional propagation towards the equator and for guiding the waves upward towards the vertical reflecting surface and subsequently back downwards towards the troposphere.

b. Northern hemisphere

Given the importance of meridional wave guiding in the southern hemisphere we also examine its role in the northern hemisphere. As discussed in the Introduction, Perlwitz and Harnik (2003) investigated wave-one reflection during JFM and SON (3-month average periods) in the northern hemisphere using NCEP-NCAR reanalysis data from 1979 to 2001. They argued that an index based on a vertical reflecting surface was useful for isolating years with downward wave coupling. In the previous section it was shown that in the southern hemisphere the presence of a vertical reflecting surface is not a sufficient criteria for downward

wave coupling (cf. winter in the southern hemisphere). Since Perlwitz and Harnik (2003, 2004) only investigated wave reflection during fall and mid-to-late winter, we investigate the full seasonal cycle of downward wave coupling and wave geometry. We repeat all of the diagnostics from the previous subsection.

Figure 6 shows the seasonal evolution based on two-month overlapping periods from September to May of the wave-one cross-correlations with a reference latitude band from 45 to 80°N at 500 hPa with vertical levels from 1000 to 1 hPa for time lags between -10 and 10 days. There is significant upward planetary wave propagation (significant correlations for positive lags) from September to March. In general the correlations for positive lags in the northern hemisphere are statistically significant over a wider range of time lags than those in the southern hemisphere. Figure 7 shows the vertical phase structure in November-December (left panel) and February-March (right panel) for +6 day lag (dashed line). The upward propagation for positive lags is confirmed by the vertical phase structure from representative two months periods. The phase tilt is westward with height above 500 hPa in both November-December and February-March, which indicates upward wave propagation.

In the northern hemisphere the seasonal cycle of the cross-correlations associated with downward wave propagation (correlations for negative time lags in Fig. 7) have a similar evolution as those in the southern hemisphere except that they occur two months earlier in the seasonal cycle. The shift in the seasonal evolution of the correlations between the two hemispheres is consistent with the fact that planetary waves are stronger in the northern hemisphere. Note that the downward wave correlations during April-May are not accompanied by significant upward correlations. Thus, we assume that during April-May the coupling will be dominated by different dynamics related to the final vortex breakdown in

particular nonlinear wave dynamics and reflection from a critical surface rather than simple linear reflection from a vertical reflecting surface. Figure 7 shows that the phase tilt for the -6 day lag correlation (solid line) is eastward with height above 500 hPa in both November-December and February-March, which confirms that the negative time lags are associated with downward wave propagation. The phase tilt with height in both November-December and February-March is very smooth and not indicative of a standing wave pattern as found in the southern hemisphere during October-November.

Figure 8 (top panel) shows the climatological seasonal cycle of the zonal wave-one vertical wavenumber averaged between 55 and 75°N along with zonal-mean cross sections of the meridional wavenumber during November-December (bottom left panel) and February-March (bottom right panel). As in the southern hemisphere, there are two times during the year when there is a vertical reflecting surface in the stratosphere: early winter (November-December) and late winter (February-March). The vertical reflecting surface is very high in the stratosphere in November-December and very low from March onwards. In November-December and February-March the vertical reflecting surface extends from 1 to 3 hPa, however the vertical reflecting surface in November-December extends further south than that in February-March (Fig. 8 bottom panels). The seasonal cycle of the vertical wavenumber agrees with the results of Perlwitz and Harnik (2003): the three-month JFM average clearly has a vertical reflecting surface where as the three-month SON average does not. We know from Perlwitz and Harnik (2003) that the vertical reflective surface during JFM is not a permanent reflective surface, it is associated with the interannual variability of the stratospheric jet, which results from major stratospheric sudden warming events.

The lack of downward wave coupling during November-December despite the presence of

a vertical reflecting surface can once again be understood using the meridional wavenumber. Figure 9 (top panel) shows the climatological seasonal cycle of the zonal wave-one meridional wavenumber averaged between 100 and 30 hPa along with zonal-mean cross sections of the meridional wavenumber during November-December (bottom left panel) and February-March (bottom right panel). Overlying the seasonal cycle of l is the seasonal cycle of m averaged between 3 to 1 hPa. As in the southern hemisphere there is a very wide meridional wave guide throughout most of the year (April to December). This wide meridional wave guide allows for meridional propagation into the subtropics where the waves would encounter a subtropical critical surface. From January to March however, there is a well-defined high-latitude meridional wave guide from approximately 45 to 75°N. In February-March the climatological wave geometry is not completely bounded as it is during October-November in the southern hemisphere (compare the bottom right panels in Figs. 9 and 4). However, there is still a high-latitude meridional wave guide, which is important for focusing wave energy in the vertical. Perlwitz and Harnik (2003) showed that downward wave coupling during individual JFM months is associated with a bounded wave geometry (see their Figs. 12c,d).[2]

Finally, we confirm that meridional wave guiding is important for focusing planetary wave propagation in the vertical direction by considering the seasonal cycle of wave one EP fluxes. Figure 10 shows the climatological seasonal cycle of the ratio of the wave one

[2]Perlwitz and Harnik (2003) created an index for downward wave coupling based on the difference of the zonal wind at 2 and 10 hPa averaged between 58-74°N. The index was used by Perlwitz and Harnik (2004) to separate years with and without wave coupling. Our results suggest that a wave coupling index should be based on both m and l.

meridional component of the EP flux at 35°N averaged between 100 and 10 hPa to the vertical flux at 100 hPa averaged between 35 and 90°N (solid line) from October to April. This ratio has a negative trend from early to late winter (November-April) though the trend is weaker than that in the southern hemisphere. However, there is still an indication that for a given amount of vertical flux through 100 hPa there is more meridional flux through 35°N during November-December than during February-March, consistent with the meridional wavenumber evolution. Figure 10 also shows the ratio of the vertical flux at 10 hPa and the vertical flux at 100 hPa both averaged between 35 and 90°N (dashed line). This ratio is nearly constant (with wave pulses which likely reflect the large variability and insufficient data to properly capture the climatology), which is consistent with the existence of downward wave reflection during November to March. However the relative amount of wave reflection is overall much smaller in the northern hemisphere than in the southern hemisphere (compare Figs. 5 and 10). The decrease in the ratio in April-May is consistent with the breakup of the polar vortex and a downward progression of the critical surface for stationary waves, which prevents the waves from reaching 10 hPa. Note that the sum of the two EP ratios is never greater than one, which indicates that the stratosphere is not a source of wave one as it was in the southern hemisphere. Overall, the EP flux ratio diagnostics support the hypothesis that a high-latitude meridional wave guide plays an important role in downward wave coupling in both hemispheres.

4. The relative role of wave versus zonal-mean coupling in the seasonal cycle

The previous section showed that the seasonal evolution of downward wave coupling and wave geometry for wave one in the southern and northern hemispheres are similar in many respects. However, there are also important differences. First, the phase structure of the downward propagating wave is different in the two hemispheres. In the southern hemisphere the cross-correlations and phase for negative lags were suggestive of a standing wave pattern and indicative of a wave in the presence of a permanent vertical reflecting surface. In the northern hemisphere, however the phase tilt with height was not suggestive of a standing wave. This is most likely due to the interannual variability in downward wave coupling in the northern hemisphere. Second, the cross-correlations for upward propagating waves in the northern hemisphere are statistically significant over a broader range of time lags than those in the southern hemisphere (compare the correlations for positive time lags in Fig. 1 to Fig. 6). This suggests a longer time scale of the upward planetary wave activity pulses in the northern hemisphere, which can be seen in the EP flux ratios (compare Fig. 5 to Fig. 10). Harnik (2009) found that the time duration of the upward planetary wave activity pulse entering the stratosphere from the troposphere is an important factor determining whether planetary waves are reflected or absorbed. In particular short (long) pulses were preferentially reflected (absorbed). Wave absorption is analogous to wave dissipation and induces a downward propagating zonal-mean response and zonal-mean stratosphere-troposphere coupling. Overall, these differences between the hemispheres suggest that the relative importance of intraseasonal downward wave and zonal-mean stratosphere-troposphere coupling is

different between the hemispheres.

A common diagnostic for quantifying the zonal-mean coupling between the stratosphere and troposphere is time-lagged correlations of the northern and southern annular mode (NAM, SAM) time series at 10 hPa with all vertical levels. Baldwin and Dunkerton (1999) and Perlwitz and Harnik (2004) computed time-lagged correlations of the NAM index and Thompson et al. (2005) computed similar correlations for the SAM index. Christiansen (2001) used the zonal-mean zonal wind at 60°N and 60°S to calculate downward zonal-mean correlations in the extratropical northern and southern hemispheres. The zonal-mean coupling is identified by enhanced correlations for positive time lags exceeding a few days. Here we use the SAM and NAM index correlations to assess intraseasonal zonal-mean coupling and compare it to the downward wave coupling between the stratosphere and troposphere. The SAM and NAM indices at each pressure level were determined by applying an empirical orthogonal function analysis on zonal-mean geopotential height data south of 20°S and north of 20°N, respectively (Baldwin and Thompson 2009).

Figure 11 (left panel) shows the seasonal cycle based on two-month overlapping periods of the time-lagged correlations of the SAM index between 20 hPa and 1000 hPa (shaded contours) and the wave-one cross-correlations between 20 hPa and 500 hPa averaged from 45 to 80°S (solid contours) for time lags between -30 and +30 days. Here we use the 20 hPa level as reference level. The 20 hPa/1000 hPa and 20 hPa/500 hPa level combinations were selected because the zonal-mean and wave-one correlations maximize at those levels, respectively. The SAM data were high-pass filtered to remove all variability greater than one year so as to remove the interannual variability associated with changes in the timing of polar vortex breakdown in the stratosphere, which could dominate the zonal-mean correlations

between the stratosphere and troposphere in spring. The wave-one cross-correlations from April to December in Fig. 11 are identical to the correlations at 20 hPa in Fig. 1 except that the time lags are reversed. During summer the wave-one cross-correlations maximize between 0 and -1 day lag and are not associated with upward wave propagation but rather with hydrostatic balance in the column. During winter and spring the wave-one cross-correlations for negative time lags shift to -3 to -4 day lag and are associated with upward wave propagation. Downward wave propagation (solid contours for positive lags), occurs from September to December as discussed in section 3. The seasonal cycle of the SAM index correlations (shaded contours) suggest that the zonal-mean coupling is weak throughout the seasonal cycle. The largest SAM correlations occur near zero time lag which is more indicative of instantaneous coupling than downward migrating wave-mean flow interactions. The clear separation between the wave-one cross-correlations and SAM-index correlations in the seasonal cycle suggests that zonal-mean and downward wave coupling are distinct and dominate during different times of the year. Figure 11 (right panel) also shows the SAM index correlations (shaded contours) and the wave-one cross-correlations (solid contours) for a 20 hPa reference level as a function of height averaged from September to December (right panel). From September to December the SAM index correlations are large above 200 hPa but do not extend below 200 hPa. The wave-one cross-correlations however maximize around 500 hPa. It is clear that downward wave coupling dominates the downward coupling between the stratosphere and troposphere in the southern hemisphere during spring. Zonal-mean coupling during this time is very weak. This is consistent with the shorter time scale of the upward planetary wave activity pulses (Harnik 2009).

The corresponding seasonal evolution of time-lagged correlations of the NAM index is

shown in Figure 12 (left panel). The wave-one cross-correlations from September to May in Fig. 12 are identical to the correlations at 20 hPa in Fig. 6 except that the time lags are reversed because we use 20 hPa level as a reference level here. During summer the wave-one cross-correlations maximize between -1 and -2 day lag and are not associated with upward wave propagation. During winter and spring the wave-one cross-correlations show a clear transition from instantaneous coupling to upward propagation as the correlations for negative time lags in winter maximize between -5 to -6 day lag. Downward wave propagation (solid contours for positive lags), occurs from December to May as discussed in section 3b. The seasonal cycle of the NAM index correlations (shaded contours) shows significant zonal-mean coupling during the same time period. The time scales of coupling extend beyond 15 days. The zonal-mean coupling in the northern hemisphere is likely due to stratospheric sudden warmings, which represent strong variations in the NAM on intraseasonal time scales. Figure 12 (right panel) shows the NAM index correlations (shaded contours) and the wave-one cross-correlations (solid contours) for a 20 hPa reference level as a function of height averaged from December to March. During the active period the NAM index correlations extend below 200 hPa and are largest in the troposphere right at the surface for time lags up to 20 days consistent with previous studies (e.g. Baldwin and Dunkerton 1999). The NAM correlations in the mid-troposphere are weak. The downward wave coupling indicated by significant cross correlations at negative time lags maximizes around 500 hPa. Clearly both zonal-mean and wave processes contribute to downward coupling during northern hemisphere winter consistent with the results of Perlwitz and Harnik (2003). Perlwitz and Harnik (2004) suggested that these processes are more exclusive in their downward impact when investigating individual years. The significant contribution of zonal-mean processes is consistent

with the longer time scale of the upward planetary wave activity pulses (Harnik 2009).

5. Summary and discussion

We have examined downward wave-one coupling between the stratosphere and troposphere in the southern and northern hemispheres using the ERA-40 reanalysis data set. Wave coupling was identified using the cross-spectral correlation analysis of Randel (1987), which isolates upward and downward propagating wave signals. In particular, statistically significant cross-correlations for time lags when the stratosphere leads the troposphere indicates downward wave coupling between the two layers. The seasonal cycle of the vertical and meridional wavenumbers were calculated using the diagnostic of Harnik and Lindzen (2001) and used to locate vertical reflecting surfaces and meridional wave guides in the basic state flow in order to understand the wave propagation. Finally, SAM and NAM time-lagged correlations between different vertical levels were compared with wave-one cross-correlations to understand the relative roles of zonal-mean and downward wave coupling between the stratosphere and troposphere throughout the seasonal cycle.

In both the southern and northern hemispheres, downward wave-one coupling occurs when there is a preferred configuration of the stratospheric jet, which is associated with a high-latitude meridional wave guide and a vertical reflecting surface. In the southern hemisphere this wave geometry forms during September to December as part of the seasonal cycle and is bounded (i.e. the high-latitude meridional wave guide is bounded above by the vertical reflecting surface). In the northern hemisphere there is a high-latitude meridional wave guide and a vertical reflecting surface, and hence significant downward wave coupling, from

January to March. However, the climatological wave geometry is not completely bounded because a bounded wave geometry forms as part of the interannual variability.

In both hemispheres a vertical reflecting surface also forms during early winter, however there is no high-latitude meridional wave guide and no significant downward wave coupling. In the absence of a high-latitude meridional wave guide the waves can propagate meridionally towards the subtropics where they are absorbed near the critical surface decreasing the likelihood of downward wave coupling. Thus, the lack of a high-latitude meridional wave guide explains the lack of significant downward wave coupling during early winter. An enhancement of meridional propagation in the absence of a high-latitude meridional wave guide was confirmed in both hemispheres using Eliassen-Palm flux diagnostics.

Perlwitz and Harnik (2003) previously noted the importance of the wave geometry for wave reflection during JFM but they emphasized the importance of a vertical reflecting surface. Here we have shown that a wave geometry involving both a vertical reflecting surface and a high-latitude meridional wave guide is a general condition required for downward wave coupling between the stratosphere and troposphere in both hemispheres. This leads to the distinction between wave reflection in general, which requires a vertical reflecting surface, and downward wave coupling, which requires both a vertical reflecting surface and a high-latitude meridional wave guide.

The analysis of the relative roles of zonal-mean and downward wave coupling during the seasonal cycle revealed that in the southern hemisphere downward wave coupling dominates during spring. The intraseasonal zonal-mean coupling maximizes in winter and is very weak. The dominance of downward wave coupling in the southern hemisphere is consistent with the shorter time scale of planetary wave activity pulses (Harnik 2009). In the

northern hemisphere, both downward wave and zonal-mean coupling contribute to intraseasonal stratosphere-troposphere coupling. From December to March, downward wave coupling maximizes in the mid-troposphere (at 500 hPa) while zonal-mean coupling maximizes at the surface. The results are consistent with Perlwitz and Harnik (2004), who focused on stratosphere-troposphere coupling during JFM. They also showed that zonal-mean and downward wave coupling dominate during different years.

Our study suggests that a proper representation of the seasonal cycle of the basic state structure (i.e. the stratification, the position of the jet maximum and the critical surface, which affect the vertical and meridional wave numbers) is crucial for obtaining the correct downward wave coupling in an atmospheric general circulation model. The inability of current state-of-the-art climate models to capture the seasonal cycle of annular mode coupling between the stratosphere and troposphere (Gerber et al. 2008, 2010) may be caused in part by biases in the intraseasonal variability of downward wave coupling associated with biases in the wave geometry. An inter-model comparison of downward wave coupling and wave geometry is currently in progress.

Our analysis focused on dynamical coupling between the stratosphere and troposphere on intraseasonal time scales. In the northern hemisphere, stratosphere-troposphere coupling is characterized by large variability on the interannual and interdecadal time scales (e.g., Christiansen 2003). In the southern hemisphere, a one-month delay in the break up of the stratospheric polar vortex (Neff 1999; Waugh et al. 1999; Karpetchko et al. 2005) and a pronounced shift toward a positive SAM index (Thompson and Solomon 2002) have been observed since 1979. These changes are most likely caused by stratospheric polar ozone depletion (Gillett and Thompson 2003; Perlwitz et al. 2008). In addition, Neff et al. (2008)

noted non-zonal decadal variability around the coast of Antarctica in the troposphere and Lin et al. (2009) noted non-zonal trends in stratospheric temperature and ozone from 1979 to 2007. The causes for these non-zonal trends are not well understood. Extending the current analysis to include the effects of interannual and interdecadal variability as well as the influence of anthropogenic climate forcings (such as increases in greenhouse gas concentration and ozone depletion and recovery) on the basic state in order to better understand their effects on downward wave coupling between the stratosphere and troposphere is work in progress.

Acknowledgments.

We thank ECMWF for providing the ERA-40 reanalysis data set. This research has been supported by the Natural Sciences and Engineering Research Council of Canada through a Post Doctoral Fellowship to the first author. JPs contribution was funded by the NOAA Climate Program Office. NHs contribution was funded by grant 1370/08 from the Israeli Science Foundation. The authors are also grateful to two anonymous reviewers for helping to improve the manuscript.

REFERENCES

Baldwin, M. P. and T. J. Dunkerton, 1999: Downward propagation of the arctic oscillation from the stratosphere to the troposphere. *J. Geophys. Res.*, **104**, 30 937–30 946.

Baldwin, M. P. and T. J. Dunkerton, 2001: Stratospheric harbingers of anomalous weather regimes. *Science*, **294**, 581–584.

Baldwin, M. P., D. B. Stevenson, D. D. W. Thompson, T. J. Dunkerton, A. J. Charlton, and A. O'Neill, 2003: Stratospheric memory and skill of extended-range weather forecasts. *Science*, **301**, 636–640.

Baldwin, M. P. and D. W. J. Thompson, 2009: A critical comparison of stratosphere-troposphere coupling indices. *Q. J. R. Meteorol. Soc.*, **135**, 1661–1672.

Charney, J. G. and P. G. Drazin, 1961: Propagation of planetary disturbances from the lower into the upper atmosphere. *J. Geophys. Res.*, **66**, 83–109.

Christiansen, B., 2001: Downward propagation of zonal mean zonal wind anomalies from the stratosphere to the troposphere: Model and reanalysis. *J. Geophys. Res.*, **104**, 30 937–30 946.

Christiansen, B., 2003: Evidence for nonlinear climate change: Two stratospheric regimes and a regime shift. *J. Climate*, **16**, 3681–3689.

Gerber, E. P., L. Polvani, and D. Ancukiewicz, 2008: Annular mode time scales in the Intergovernmental Panel on Climate Change Fourth Assessment Report models. *Geophys. Res. Lett.*, **35**, doi:10.1029/2008GL035712.

Gerber, E. P., et al., 2010: Stratosphere-troposphere coupling and annular mode variability in chemistry-climate models. *J. Geophys. Res.*, in press.

Gillett, N. P. and D. W. J. Thompson, 2003: Simulation of recent southern hemisphere climate change. *Science*, **302**, 273–275.

Harnik, N., 2009: Observed stratospheric downward reflection and its relation to upward pulses of wave activity. *J. Geophys. Res*, **114**, doi:10.1029/2008JD010493.

Harnik, N. and R. S. Lindzen, 2001: The effect of reflecting surfaces on the vertical structure and variability of stratospheric planetary waves. *J. Atmos. Sci.*, **58**, 2872–2894.

Karpetchko, A., E. Kyrö, and B. M. Knudsen, 2005: Arctic and antarctic polar vortices 19572002 as seen from the ERA-40 reanalyses. *J. Geophys. Res.*, **110**, doi:10.1029/2005JD006113.

Lin, P., Q. Fu, S. Solomon, and J. M. Wallace, 2009: Temperature trend patterns in the southern hemisphere high latitudes: Novel indicators of stratospheric change. *J. Climate*, **22**, 6325–6341.

Neff, W., 1999: Decadal time scale trends and variability in the tropospheric circulation over the south pole. *J. Geophys. Res.*, **104**, 27 217–27 251.

Neff, W., J. Perlwitz, and M. Hoerling, 2008: Observational evidence for asymmetric changes

in tropospheric heights over Antarctica on decadal time scales. *Geophys. Res. Lett.*, **35**, doi:10.1029/2008GL035074.

Perlwitz, J. and N. Harnik, 2003: Observational evidence of a stratospheric influence on the troposphere by planetary wave reflection. *J. Climate*, **16**, 3011–3026.

Perlwitz, J. and N. Harnik, 2004: Downward coupling between the stratosphere and troposphere: The relative roles of wave and zonal mean processes. *J. Climate*, **17**, 4902–4909.

Perlwitz, J., S. Pawson, R. Fogt, J. E. Nielsen, and W. Neff, 2008: The impact of stratospheric ozone hole recovery on antarctic climate. *Geophys. Res. Lett.*, **35**, doi: 10.1029/2008GL033317.

Randel, W. J., 1987: A study of planetary waves in the southern winter troposphere and stratosphere. Part I: Wave structure and vertical propagation. *J. Atmos. Sci.*, **44**, 917–935.

Randel, W. J., D. E. Stevens, and J. L. Stanford, 1987: A study of planetary waves in the southern winter troposphere and stratosphere. Part II: Life cycles. *J. Atmos. Sci.*, **44**, 936–949.

Shaw, T. A. and T. G. Shepherd, 2008: Raising the roof. *Nature Geosc.*, **1**, 12–13.

Thompson, D. W. J., M. Baldwin, and S. Solomon, 2005: Stratosphere-troposphere coupling in the southern hemisphere. *J. Climate*, **62**, 708–715.

Thompson, D. W. J. and S. Solomon, 2002: Interpretation of recent southern hemisphere climate change. *Science*, **296**, 895–899.

Uppala, S., et al., 2005: The ERA-40 re-analysis. *Quart. J. Roy. Soc.*, **131**, 2961–3012.

Waugh, D. W., W. J. Randel, S. Pawson, P. A. Newman, and E. R. Nash, 1999: Persistence of the lower stratospheric polar vortices. *J. Geophys. Res.*, **104**, 27 191–27 201.

List of Figures

1 Vertical-time lag section of the correlation coherence for wave one averaged from 45 to 80°S at 500 hPa with vertical levels between 1000 and 1 hPa for two-month overlapping periods from April-May to November-December and for time lags between -10 and 10 days. Only correlations which are statistically significant at the 99% levels are contoured and the contour interval is 0.1. 35

2 The wave-one correlation phase in degrees associated with the correlation coherence in Fig. 1 for -4 (solid line) and +4 (dashed line) day time lags during May-June (left panel) and October-November (right panel). 36

3 The climatological seasonal cycle of the vertical wavenumber averaged between 55 and 75°S (top panel) and zonal-mean cross sections of the climatological vertical wavenumber in May-June (bottom left panel) and October-November (bottom right panel) in the southern hemisphere. The contours (units 10^{-5} m^{-1}) are shown at 0.01 (thick line); 2, 4 (dashed line); and 6-30 in jumps of 3 (solid). Shading indicates regions of wave evanescence ($m < 0$). 37

4 The climatological seasonal cycle of the meridional wavenumber averaged between 100 and 30 hPa (top panel) and zonal-mean cross sections of the climatological meridional wavenumber in May-June (bottom left panel) and October-November (bottom right panel) in the southern hemisphere. The contours interval is 1 rad^{-1} and the thick line represents the 0.01 contour. Dark shading indicates regions of wave evanescence ($l < 0$). Overlying the climatological seasonal cycle of the meridional wavenumber is the seasonal cycle of the vertical wave number averaged between 10 and 1 hPa. The light shading indicates regions of wave evanescence ($m < 0$). The dashed line shows the $m = 0.01$ m^{-1} contour. 38

5 Ratio of the climatological meridional component of the Eliassen-Palm flux at 35°S integrated between 100 and 10 hPa to the climatological vertical component at 100 hPa integrated between 35 and 90°S (solid line) and the ratio of the vertical component at 10 hPa integrated between 35 and 90°S to the vertical component at 100 hPa integrated between 35 and 90°S (dashed line) from June to December. The integrated flux components were smoothed with a 10-day running average. 39

6 Vertical-time lag section of the correlation coherence for wave one averaged from 45 to 80°N at 500 hPa with vertical levels between 1000 and 1 hPa for two-month overlapping periods from October-November to April-May and for time lags between -10 and 10 days. Contours and significance as in Fig. 1. 40

7 The wave-one correlation phase in degrees associated with the correlation coherence in Fig. 6 for -6 (solid line) and +6 (dashed line) day time lags during November-December (left panel) and February-March (right panel). 41

8 The climatological seasonal cycle of the vertical wavenumber averaged between 55 and 75°N (top panel) and zonal-mean cross sections of the climatological vertical wavenumber in November-December (bottom left panel) and February-March (bottom right panel) in the northern hemisphere. Contours and shading as in Fig. 3. 42

9 The climatological seasonal cycle of the meridional wavenumber averaged between 100 and 30 hPa (top panel) and zonal-mean cross sections of the climatological meridional wavenumber in November-December (bottom left panel) and February-March (bottom right panel) in the northern hemisphere. Dark shading indicates regions of wave evanescence ($l < 0$). Overlying the climatological seasonal cycle of the meridional wavenumber is the seasonal cycle of the vertical wave number averaged between 3 and 1 hPa. The light shading indicates regions of wave evanescence ($m < 0$). Contours as in Fig. 4. 43

10 Ratio of the climatological meridional component of the Eliassen-Palm flux at 35°N integrated between 100 and 10 hPa to the climatological vertical component at 100 hPa integrated between 35 and 90°N (solid line) and the ratio of the vertical component at 10 hPa integrated between 35 and 90°N to the vertical component at 100 hPa integrated between 35 and 90°N (dashed line) from October to April. The integrated flux components were smoothed with a 10-day running average. 44

11 The climatological seasonal cycle for two-month overlapping periods of the time-lagged correlation of the SAM index between 20 hPa and 1000 hPa (shaded) and the wave one cross-coherence correlations between 20 hPa and 500 hPa both averaged from 45 to 80°S (solid lines) for time lags between -30 and 30 days (left panel). The right panel shows the time-lagged correlation of the SAM index between 20 hPa and 1000 hPa (shaded) and the wave one cross-coherence correlations between 20 hPa and 500 hPa (solid lines) from September to December. 45

12 The climatological seasonal cycle for two-month overlapping periods of the time-lagged correlation of the NAM index between 20 hPa and 1000 hPa (shaded) and the wave one cross-coherence correlations between 20 hPa and 500 hPa both averaged from 45 to 80°N (solid lines) for time lags between -30 and 30 days (left panel). The right panel shows the time-lagged correlation of the NAM index between 20 hPa and 1000 hPa (shaded) and the wave one cross-coherence correlations between 20 hPa and 500 hPa (solid lines) from December to March. 46

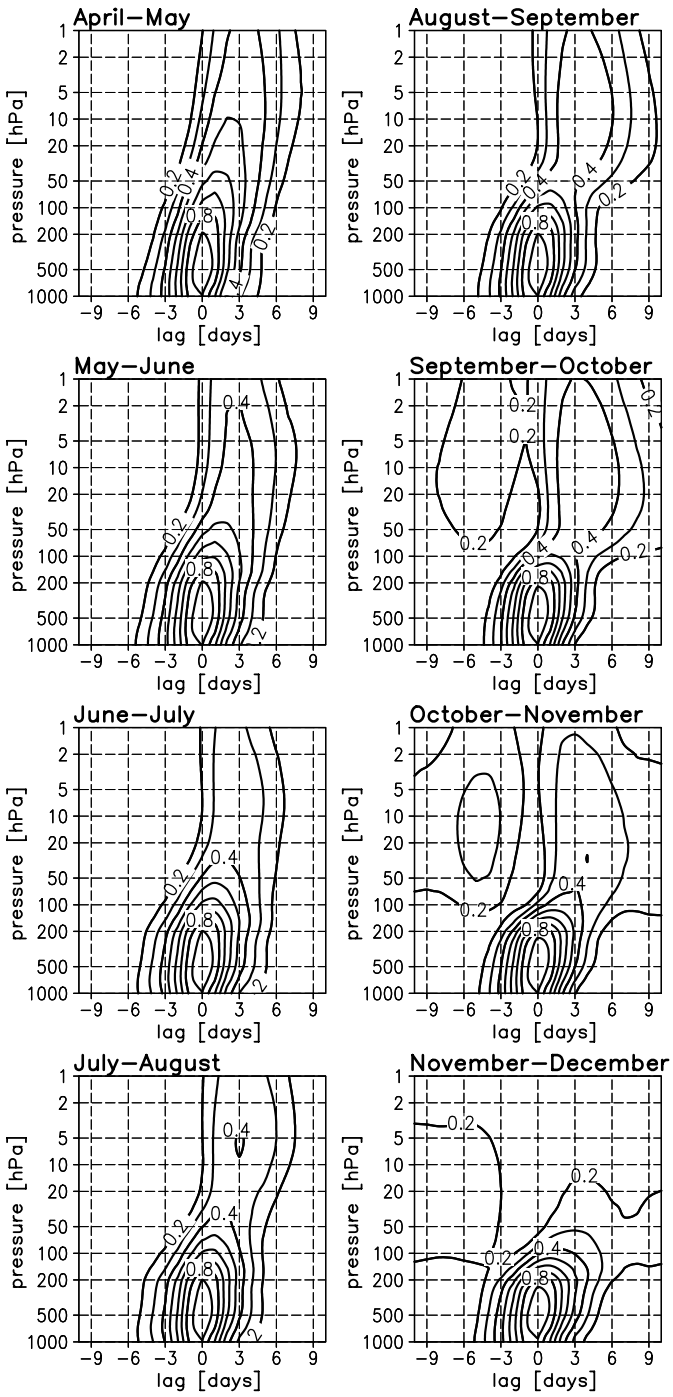

FIG. 1. Vertical-time lag section of the correlation coherence for wave one averaged from 45 to 80°S at 500 hPa with vertical levels between 1000 and 1 hPa for two-month overlapping periods from April-May to November-December and for time lags between -10 and 10 days. Only correlations which are statistically significant at the 99% levels are contoured and the contour interval is 0.1.

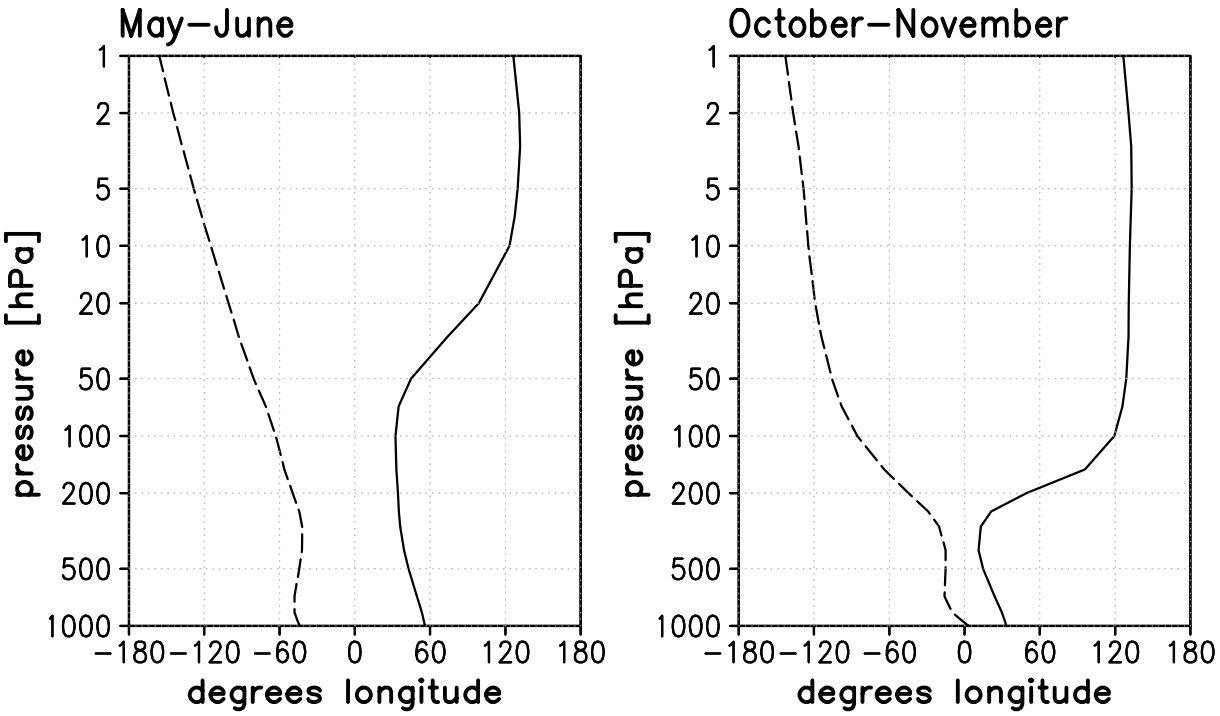

FIG. 2. The wave-one correlation phase in degrees associated with the correlation coherence in Fig. 1 for -4 (solid line) and +4 (dashed line) day time lags during May-June (left panel) and October-November (right panel).

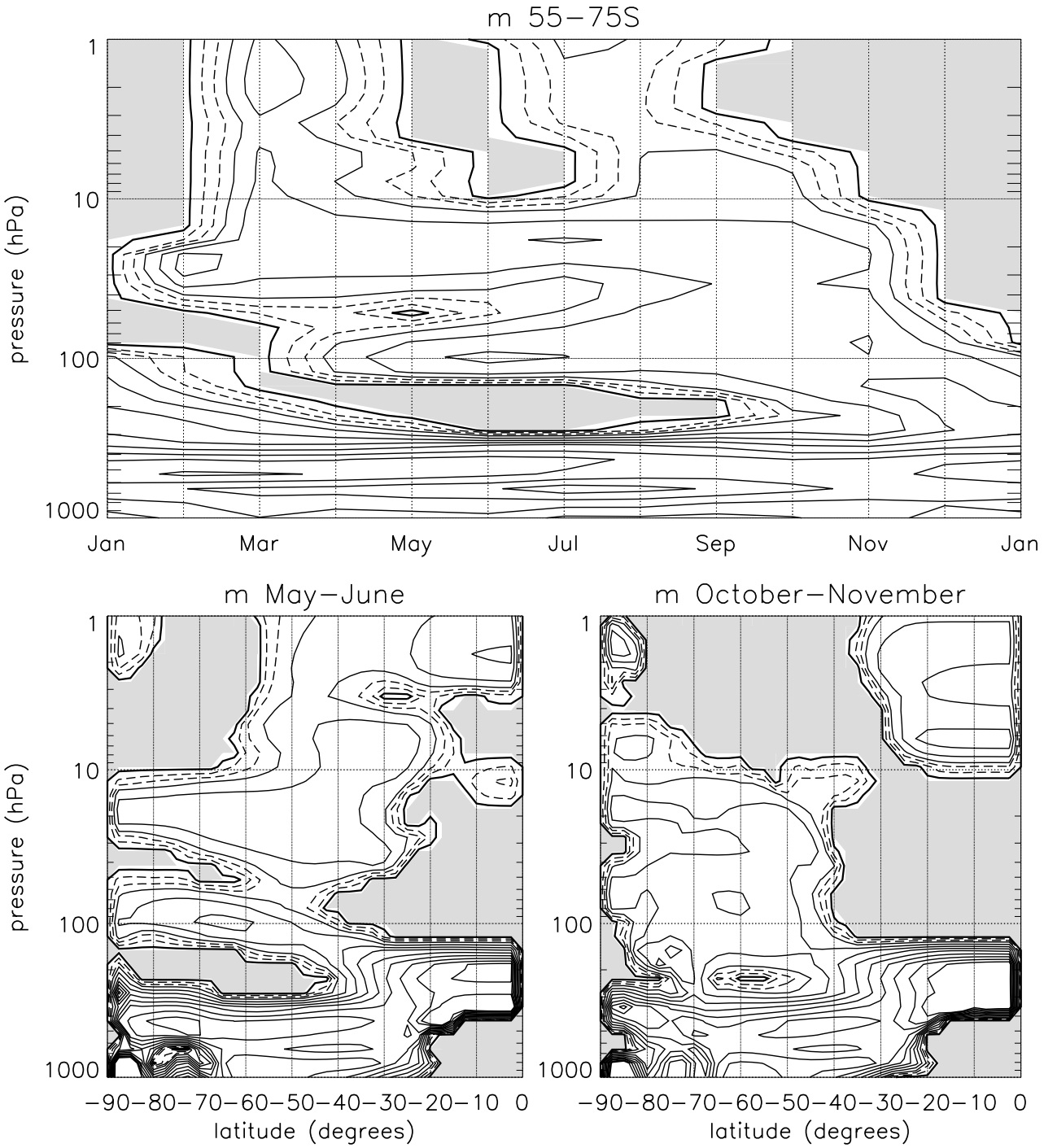

FIG. 3. The climatological seasonal cycle of the vertical wavenumber averaged between 55 and 75°S (top panel) and zonal-mean cross sections of the climatological vertical wavenumber in May-June (bottom left panel) and October-November (bottom right panel) in the southern hemisphere. The contours (units 10^{-5} m^{-1}) are shown at 0.01 (thick line); 2, 4 (dashed line); and 6-30 in jumps of 3 (solid). Shading indicates regions of wave evanescence ($m < 0$).

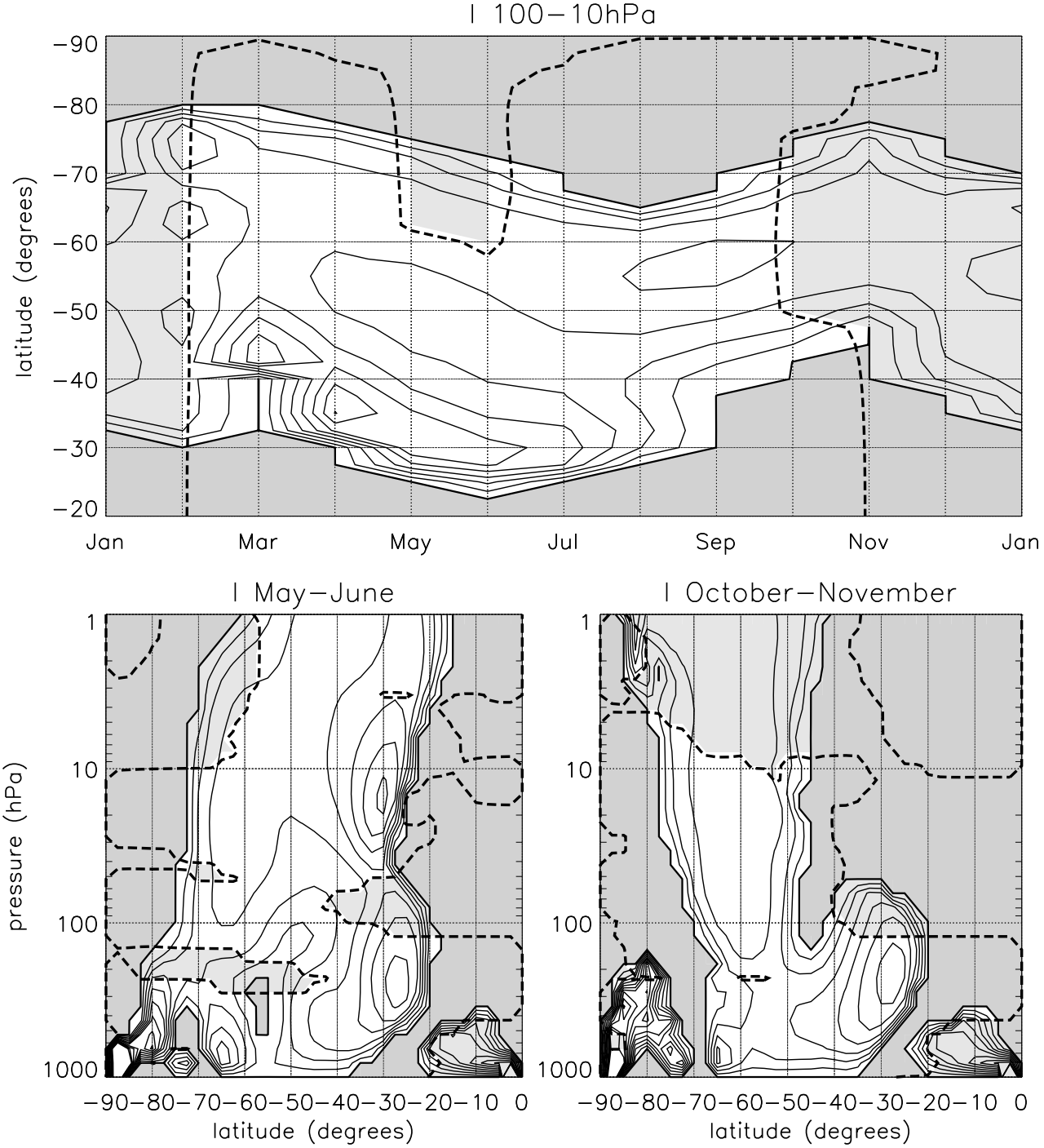

FIG. 4. The climatological seasonal cycle of the meridional wavenumber averaged between 100 and 30 hPa (top panel) and zonal-mean cross sections of the climatological meridional wavenumber in May-June (bottom left panel) and October-November (bottom right panel) in the southern hemisphere. The contours interval is 1 rad^{-1} and the thick line represents the 0.01 contour. Dark shading indicates regions of wave evanescence ($l < 0$). Overlying the climatological seasonal cycle of the meridional wavenumber is the seasonal cycle of the vertical wave number averaged between 10 and 1 hPa. The light shading indicates regions of wave evanescence ($m < 0$). The dashed line shows the $m = 0.01$ m^{-1} contour.

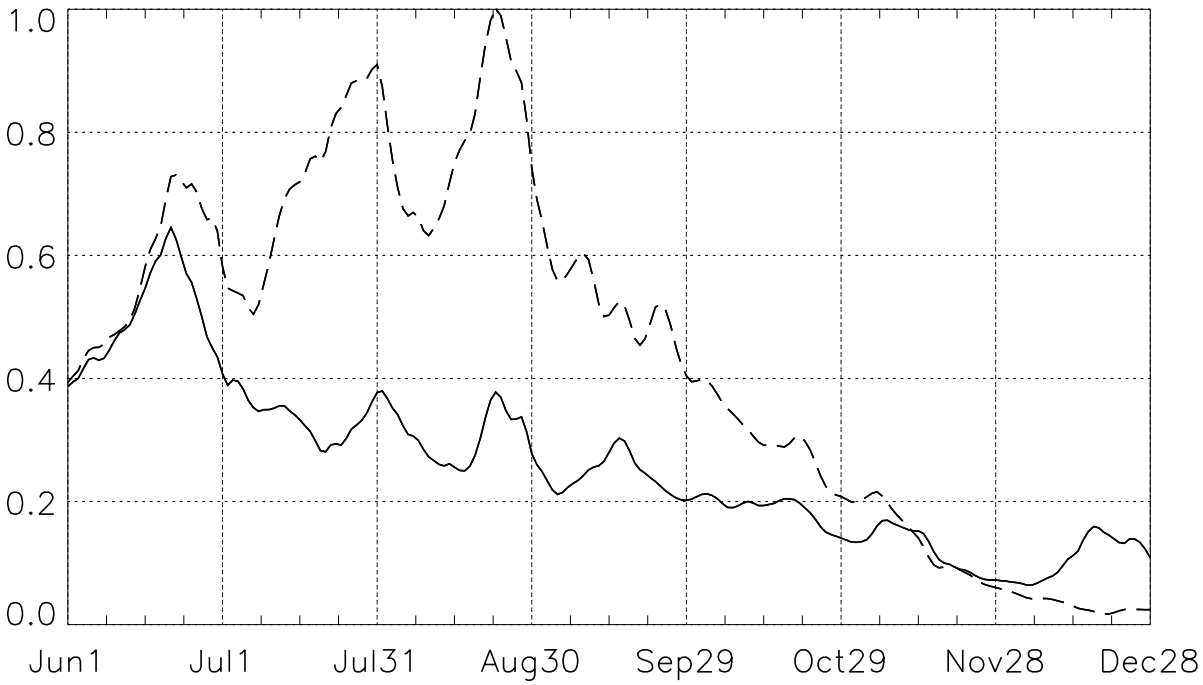

FIG. 5. Ratio of the climatological meridional component of the Eliassen-Palm flux at 35°S integrated between 100 and 10 hPa to the climatological vertical component at 100 hPa integrated between 35 and 90°S (solid line) and the ratio of the vertical component at 10 hPa integrated between 35 and 90°S to the vertical component at 100 hPa integrated between 35 and 90°S (dashed line) from June to December. The integrated flux components were smoothed with a 10-day running average.

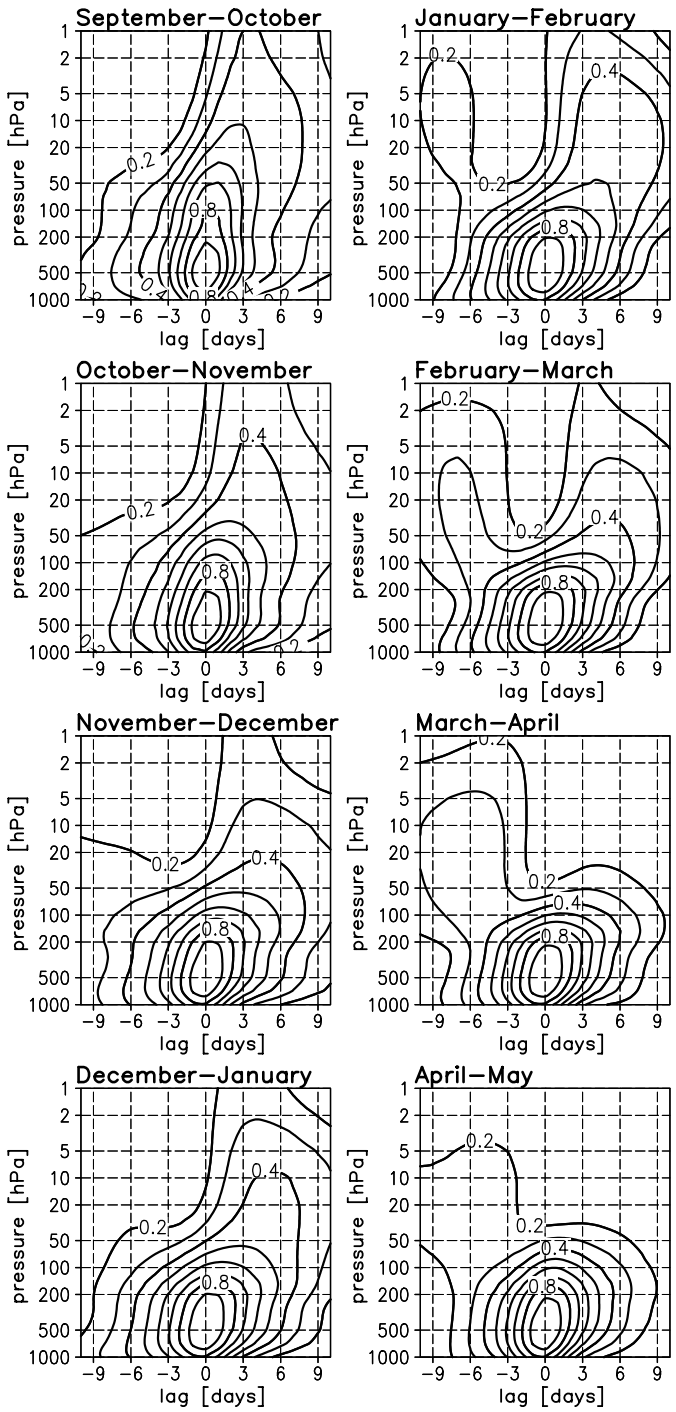

FIG. 6. Vertical-time lag section of the correlation coherence for wave one averaged from 45 to 80°N at 500 hPa with vertical levels between 1000 and 1 hPa for two-month overlapping periods from October-November to April-May and for time lags between -10 and 10 days. Contours and significance as in Fig. 1.

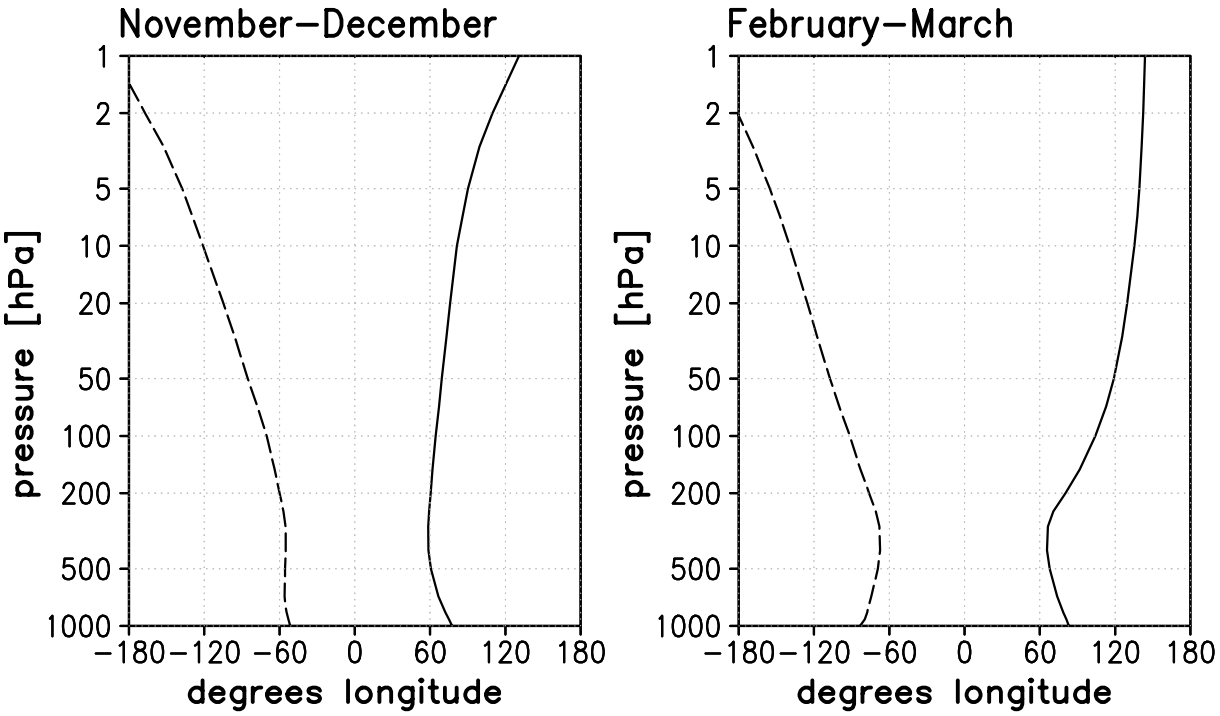

FIG. 7. The wave-one correlation phase in degrees associated with the correlation coherence in Fig. 6 for -6 (solid line) and +6 (dashed line) day time lags during November-December (left panel) and February-March (right panel).

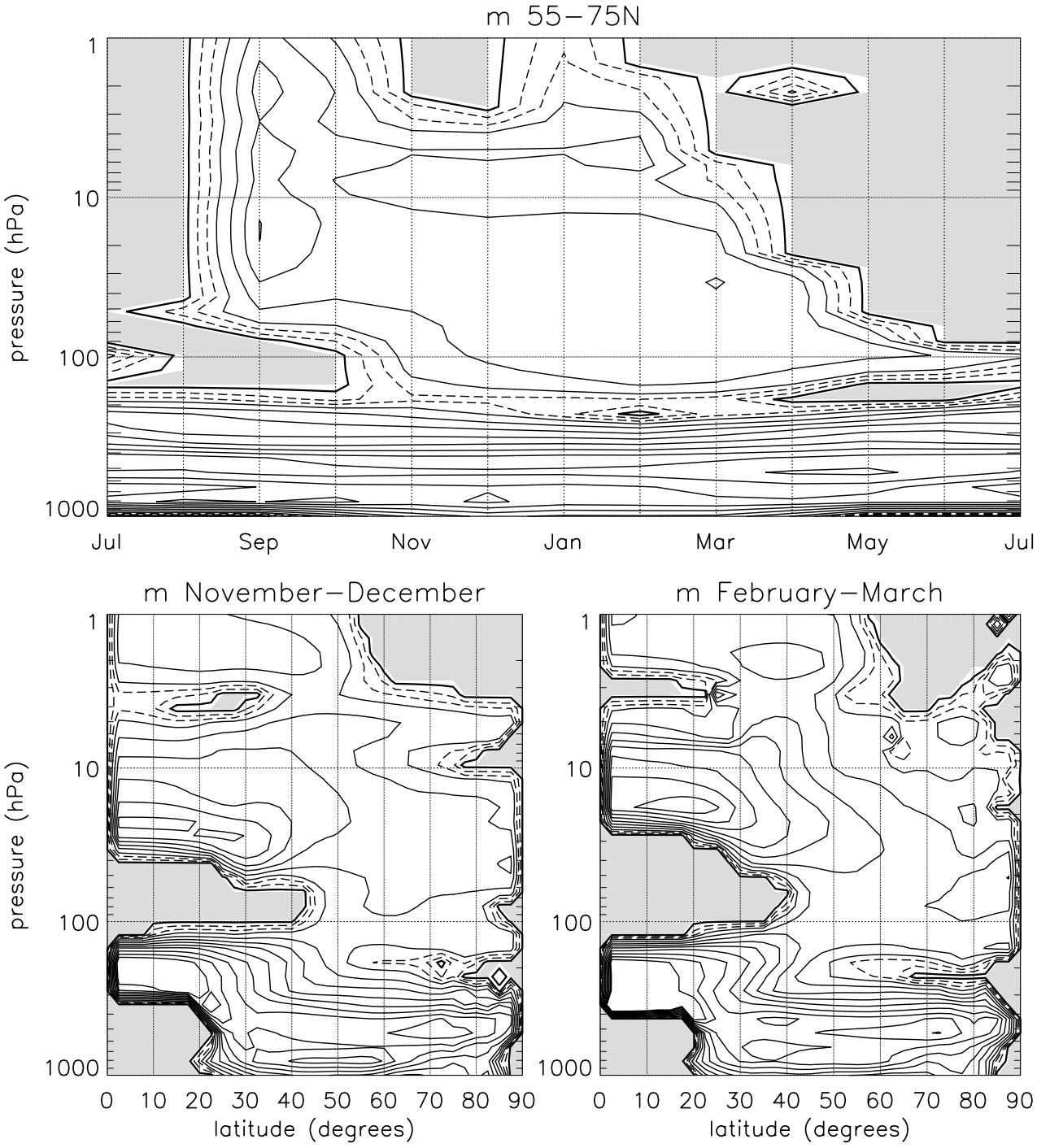

FIG. 8. The climatological seasonal cycle of the vertical wavenumber averaged between 55 and 75°N (top panel) and zonal-mean cross sections of the climatological vertical wavenumber in November-December (bottom left panel) and February-March (bottom right panel) in the northern hemisphere. Contours and shading as in Fig. 3.

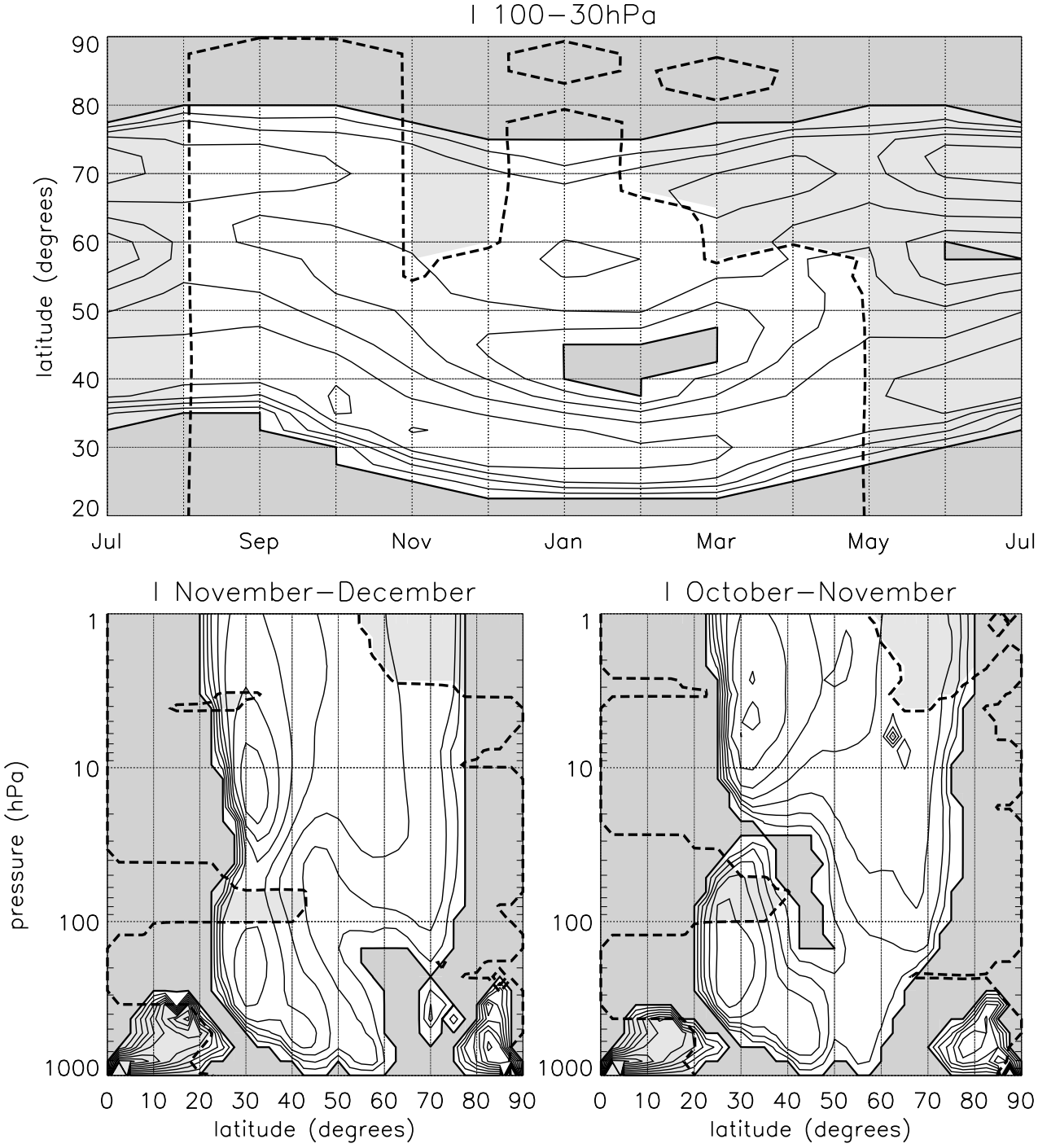

FIG. 9. The climatological seasonal cycle of the meridional wavenumber averaged between 100 and 30 hPa (top panel) and zonal-mean cross sections of the climatological meridional wavenumber in November-December (bottom left panel) and February-March (bottom right panel) in the northern hemisphere. Dark shading indicates regions of wave evanescence ($l < 0$). Overlying the climatological seasonal cycle of the meridional wavenumber is the seasonal cycle of the vertical wave number averaged between 3 and 1 hPa. The light shading indicates regions of wave evanescence ($m < 0$). Contours as in Fig. 4.

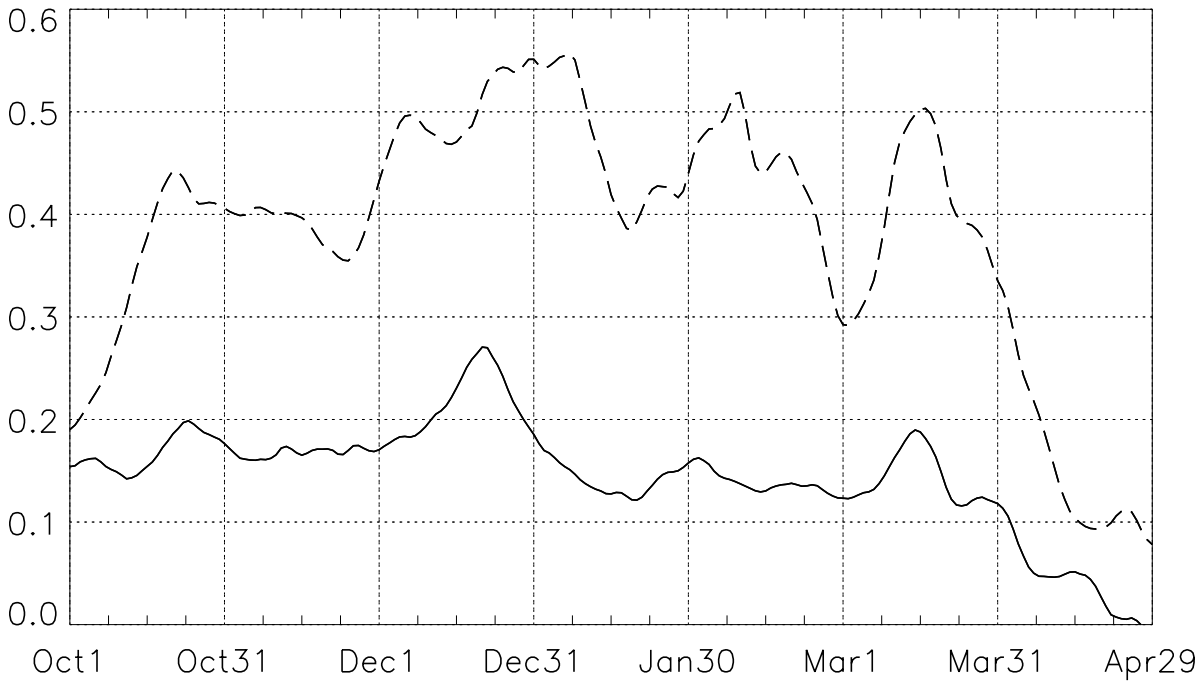

FIG. 10. Ratio of the climatological meridional component of the Eliassen-Palm flux at 35°N integrated between 100 and 10 hPa to the climatological vertical component at 100 hPa integrated between 35 and 90°N (solid line) and the ratio of the vertical component at 10 hPa integrated between 35 and 90°N to the vertical component at 100 hPa integrated between 35 and 90°N (dashed line) from October to April. The integrated flux components were smoothed with a 10-day running average.

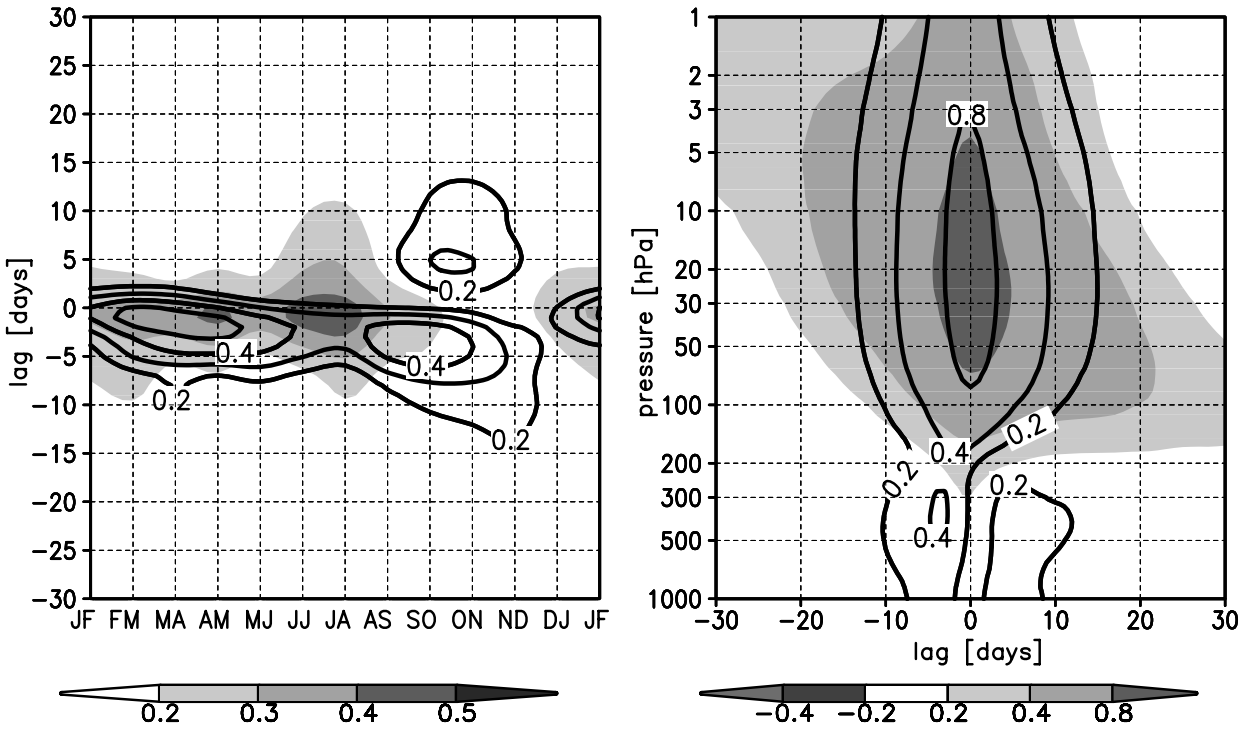

FIG. 11. The climatological seasonal cycle for two-month overlapping periods of the time-lagged correlation of the SAM index between 20 hPa and 1000 hPa (shaded) and the wave one cross-coherence correlations between 20 hPa and 500 hPa both averaged from 45 to 80°S (solid lines) for time lags between -30 and 30 days (left panel). The right panel shows the time-lagged correlation of the SAM index between 20 hPa and 1000 hPa (shaded) and the wave one cross-coherence correlations between 20 hPa and 500 hPa (solid lines) from September to December.

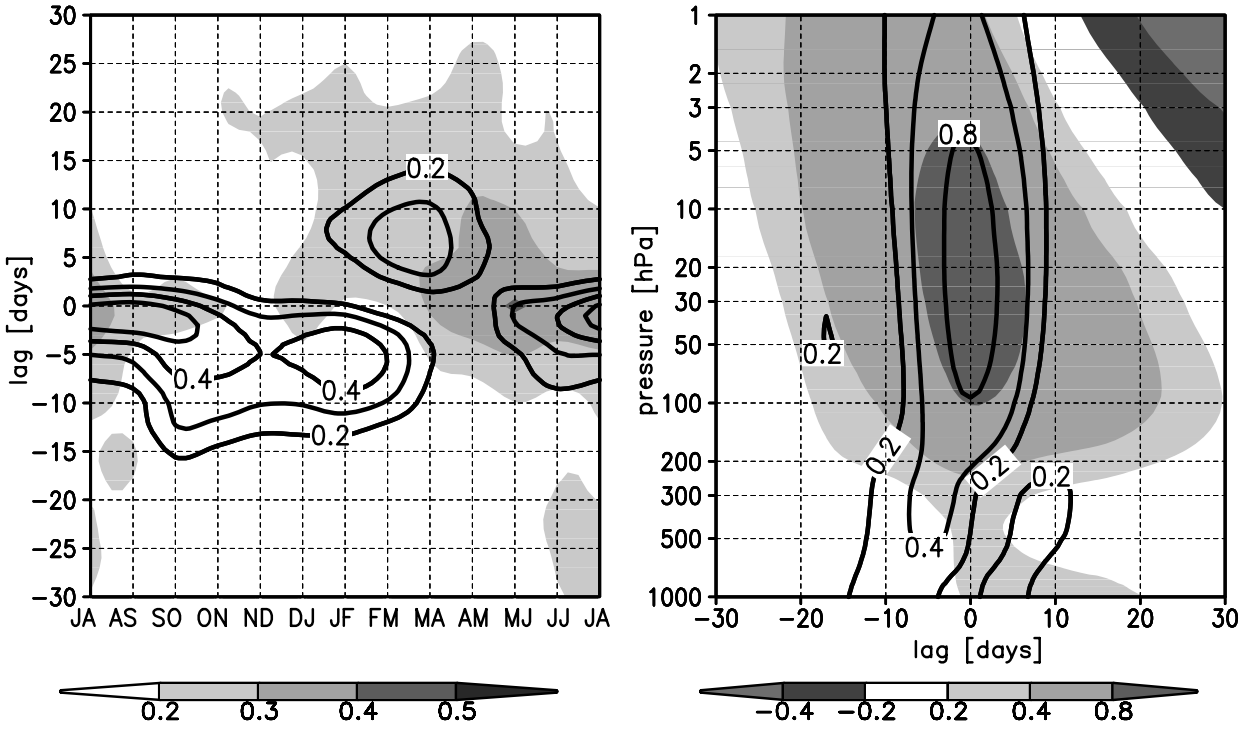

FIG. 12. The climatological seasonal cycle for two-month overlapping periods of the time-lagged correlation of the NAM index between 20 hPa and 1000 hPa (shaded) and the wave one cross-coherence correlations between 20 hPa and 500 hPa both averaged from 45 to 80°N (solid lines) for time lags between -30 and 30 days (left panel). The right panel shows the time-lagged correlation of the NAM index between 20 hPa and 1000 hPa (shaded) and the wave one cross-coherence correlations between 20 hPa and 500 hPa (solid lines) from December to March.